On the use of Vortex Generators to improve Tidal Turbine performance

Harmanvir Singh, Nicholas Kaufmann, Pablo Ouro, George Papadakis, Marinos Manolesos

Abstract—**Vortex Generators (VGs) are a passive flow control device with multiple applications, including horizontal axis wind turbines (HAWT). Their most popular version is that of thin vanes protruding normal to the blade surface, at an angle to the oncoming flow. Despite their popularity and success in the more established wind turbine industry there has been very little application of VGs on tidal turbines. The present investigation builds on the success of VGs on HAWTs and attempts to examine their effect on a tidal turbine. A numerical VG parametric study is performed on two hydrofoil profiles of different thickness, 30% and 20%. An in-house Reynolds Averaged Navier Stokes solver (MaPFlow) is used for this part of the study. The best performing VG configurations are selected and their effect on the profiles' lift and drag polars are used to predict the effect on the tidal turbine performance. This is evaluated using an in-house Blade Element Momentum code. Results are very promising and indicate that the use of VGs could significantly improve the performance of tidal turbines over a range of tip speed ratios. Future work includes wind tunnel tests to further validate the present simulations, blade resolved RANS analysis of the turbine blade and high-fidelity simulations to analyse the VG effect on the boundary layer flow.**

Keywords—**Vortex Generator, Tidal Turbine, Reynolds Averaged Navier Stokes, Blade Element Momentum, Flow Control**

I. Introduction

EVERY aerodynamically shaped body, experiences flow separation to a certain extent, often taking place over a range of operational envelope. The tidal turbine blades are no different. The existence of flow separation on tidal turbine blades is undesirable and leads to reduced performance [1]. This performance degradation can further manifest itself into lower annual energy production and higher fatigue loads, directly influencing the cost of energy [2].

Passive flow control methods, such as vortex generators (VGs) can reduce or even prevent the flow from separating [3]. VGs have been used in the wind turbine industry for decades [4], and the vane type has been the most popular due to its inherent simplicity and effectiveness. The operating principle is rather simple, with VGs generating streamwise vortices which bring high momentum fluid from the flow outside the boundary layer closer to the solid surface.

Tidal turbine studies [5], [6] indicate that separation occurs at the inner part of the blade, where the blade profiles are thicker, as in HAWTs. Despite this there is currently very limited research on the effect of VGs on thick hydrofoils [7] or indeed overall tidal turbine performance.

The present investigation is part of a research project that aims to transfer flow control knowledge and expertise from the wind turbine industry to the design of tidal turbines. This work considers two hydrofoil profiles of a commercial tidal turbine and performs a numerical VG parametric study. Based on the results of this study a VG configuration is selected for each profile and the performance of the turbine is estimated with and without the VGs.

The structure of the paper is as follows: In Section II the numerical methodology is presented, with details on the Computational Fluid Dynamics (CFD) approach followed for the parametric study and the Blade Element Momentum method used to predict the turbine performance. Results are given in Section III, while the paper closes with Discussion and Conclusions in Section IV.

II. Methodology

A. Vortex Generator flow simulation

1) Computational Fluid Dynamics Solver

The present numerical investigation was performed using the in house solver MaPFlow, originally developed at the National Technical University of Athens (NTUA) [8]. MaPFlow is a multi-block MPI enabled compressible unstructured finite volume, unsteady Reynolds averaged

Mr Harmanvir Singh obtained his MSc from the College of Engineering, Swansea University, Swansea, SA1 8EN, UK and was an intern with Sustainable Marine Energy Edinburgh, EH6 6QW, UK.

Dr Nicholas Kaufmann is a Tidal Turbine Engineer with Schottel Hydro GmbH, Mainzer Strasse 99, 56322 Spay/Rhin, Germany

Dr Pablo Ouro is a Research Fellow at the School of Mechanical, Aerospace and Civil Engineering, University of Manchester, Manchester, M13 9PL, UK

Dr George Papadakis is an Assistant Professor at the School of Naval Architecture & Marine Engineering, National Technical University of Athens, Athens 157 80, Greece

Dr Marinos Manolesos is a Senior Lecturer at the College of Engineering, Swansea University, Swansea, SA1 8EN, UK

Navier Stokes (URANS) solver. For space and time discretisation, the solver is second order accurate and can resolve both structured and unstructured grids. Furthermore, the discretisation technique is cell centred and for the convective fluxes, uses the Roe approximate Reimann solver for the estimation of inter cell fluxes. The solver has an in-built low Mach preconditioning for incompressible flow. In the present study, the k-ω shear stress transport (SST) [9] model was used. Steady state simulations were performed unless otherwise stated.

The presence of the VGs in the flow was modelled using the BAY model [10] in its jBAY [11] variation. This has been implemented and thoroughly validated in MaPFlow [12]–[17].

2) Computational grid

An O-shape structured computational grid was utilised for the simulations with the far-field radius of 150 chord lengths. First, a structured 2D grid was generated, which was extruded in the spanwise direction. Following a grid dependence study, the baseline 2D grid had 80000 cells. For the VG cases a local refinement at the region of the VGs was performed. The first cell height was selected so that y+ < 1 throughout the surface of the hydrofoil. The spanwise length of the computational domain was equal to D/2, see

, and 50 cells were used in the spanwise direction.

3) Validation

The numerical approach was further validated against wind tunnel data from wind turbine airfoil tests. It was decided to use a 30% thick airfoil case (DU97-W-300, [18]), as the benchmark case. This is considered more challenging compared to the lower thickness airfoil data available in the literature.

In the interest of brevity only the case with the VGs is shown here. Lift and drag coefficient comparisons are given in Fig. 2 and Fig. 3, respectively. The Cp comparison is given in Fig. 4. The agreement is considered good below stall. The disagreement for $\alpha > 16°$ is expected as Stall Cells appear in that range [18], [19]. The low aspect ratio simulations performed in this study cannot capture this large scale 3D phenomenon [20], [21].

B. Examined Cases

1) Hydrofoil Profiles

Two different hydrofoil profiles are considered in this study, one 30% thick and one 20% thick. The profiles correspond to different sections of the turbine blade and for confidentiality reasons the profiles are not given here.

2) Vortex Generators

Triangular vane VGs were used, as this is the type that is most commonly used in the wind turbine industry (see e.g. [15], [18], [22]).

For the 30% thick profile, a parametric study was performed on the VG chordwise location (x_{vg}) and VG angle (β), while the VG height (h) was always equal to the local boundary layer height (δ). The other VG parameters (L, d, D, see Fig. 1) were selected based on the literature for wind turbine airfoils [18] and for all cases the following values were used: $d = 3.5h$, $D = 7h$, $L = 3h$.

For the 20% thick profile, in addition to the VG chordwise location (x_{vg}) and the VG angle (β), the inter-vane spacing D was examined as a parameter. The other parameters remained unchanged $d = 3.5h$, $L = 3h$ and $h = \delta$.

Finally, a single case for each profile was selected for a Reynolds number dependency test in the range $0.65 \times 10^6 < Re < 2.0 \times 10^6$. Table II & III show the examined cases for each hydrofoil.

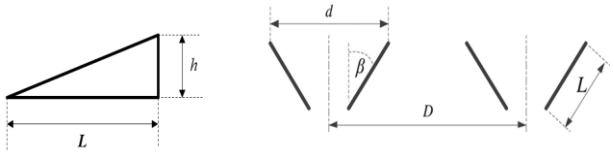

Fig. 1. VG parameters. Left: side view of a single VG; right: top view of two VG pairs with the flow coming from the bottom. Parameters shown are h, vane height, L, vane length, β, vane angle to the oncoming flow, D, inter-vane spacing, and d, intra-vane spacing.

TABLE I
DELTA VG DIMENSIONS FOR THE PARAMETRIC STUDY – 30% HYDROFOIL

Re [-]	x_{VG}/c	h [c]	β	D[h]
1×10^6	10%	0.003	+15°	7
1×10^6	20%	0.005	+10°,+15°,+20°,25°	7
1×10^6	30%	0.007	+15°	7
0.65×10^5	20%	0.005	+20°	7
2×10^6	20%	0.005	+20°	7

TABLE II
DELTA VG DIMENSIONS FOR THE PARAMETRIC STUDY – 20% HYDROFOIL

Re [-]	x_{VG}/c	h [c]	β	D[h]
1×10^6	10%	0.002	+15°	7
1×10^6	20%	0.004	+15°	7
1×10^6	30%	0.006	+15°	7
1×10^6	40%	0.009	+15°	7
1×10^6	30%	0.010	+10°,+15°,+20°,+25°	7
1×10^6	30%	0.010	+15°	7, 10.5, 14
0.65×10^5	30%	0.010	+20°	7
2×10^6	30%	0.010	+20°	7

C. Effect on Turbine Performance

1) Turbine Performance Simulation

To estimate the effect of VGs on the turbine performance an enhanced in-house blade element momentum method (BEM) solver is used. A detailed description of the solver as well as a validation based on model scale test data without VGs is given in [23].

The authors are aware that the 2D BEM method is not suitable to capture the complex, three-dimensional flow field of vortex generators. Rather, the study presented here is intended to demonstrate the potential impact of VGs on turbine performance should the change in polar data due to VGs under real operating conditions match the numerical prediction.

In order to increase the accuracy of the method, various sub-models are applied. Buhl's [24] correction of the thrust coefficient for large axial flow retardation is

used, as well as models by Prandtl/Glauert [25] and Shen [26] accounting for blade hub and tip losses. Post-stall data are extrapolated according to Viterna et al. [27]. Although Viterna's correlation is empirical and known for its limited accuracy, it ensures the needed numerical stability.

To examine the effect of the VGs, the polar data of the Blade Elements with a relative thickness between 30% and 20% are manipulated, based on the CFD results given in the Results section. As the VGs design is limited to the 30% and 20% hydrofoil shapes, the data for the intermediate sections are estimated via linear interpolation. Overall, VGs are considered up to about 30% of the blade span.

2) Turbine Type

The turbine considered in this case is SCHOTTEL's SIT250 instream turbine in its 4m-diameter rotor version. The SIT 250 is a horizontal axis instream turbine, designed as a modular turbine system utilizing one drivetrain for two rotor diameters, 4 m and 6.3 m, which can be selected based upon the varying velocity frequency distributions of different deployment sites. The larger rotor diameter is suited to lower flow speed sites, whereas the smaller rotor dimeter is suited for higher resource sites. The SIT 250 drive train is rated at the mechanical shaft, so rated power and grid-ready electrical power are P_{rated} = 85 kW and P_{el} = 70 kW respectively. Model scale tests [23] and full-scale field measurements [28], [29] have been published in the past for this model and the results have shown good agreement with the BEM predictions.

III. RESULTS

All data in this section have been normalised with respect to values of the uncontrolled case due to confidentiality reasons. For each hydrofoil, the maximum lift coefficient, the drag coefficient at $\alpha = 0°$ and the maximum lift to drag ratio value have been used as references for the respective quantities.

A. VG effect on the 30% Hydrofoil

Fig. 6, Fig. 7 and Fig. 8 show the variation of Lift, Drag and Lift to Drag ratio with and without VGs. The examined parameter in these figures is the VG chordwise location, while the VG height is equal to the local boundary layer and the VG angle is $\beta = 15°$. It appears that the hydrofoil performs best with the VGs at 20% c. Stall is delayed by 6° and maximum lift is increased by more than 40%. In terms of lift to drag ratio, which is a crucial performance factor for tidal turbines, locating VGs at 20% c leads to a maximum L/D value increase of 23% at AoA = 10°. It is noted that when the VGs are placed at 10% c, the hydrofoil performance is deteriorated as they act more as a disturbance than as an aid to the flow.

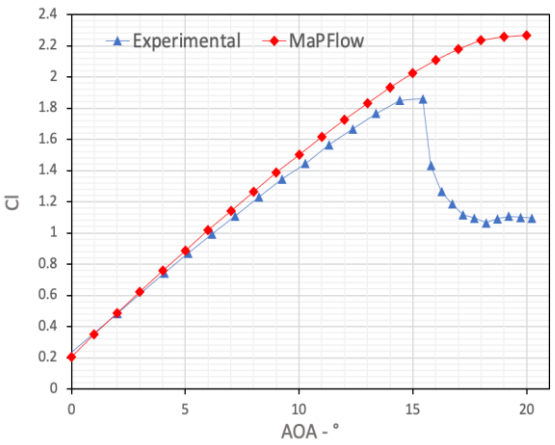

Fig. 2. Lift coefficient variation with angle of attack for the DU97-W-300 airfoil with Vortex Generators. Comparison between the present numerical approach and experimental data from [18].

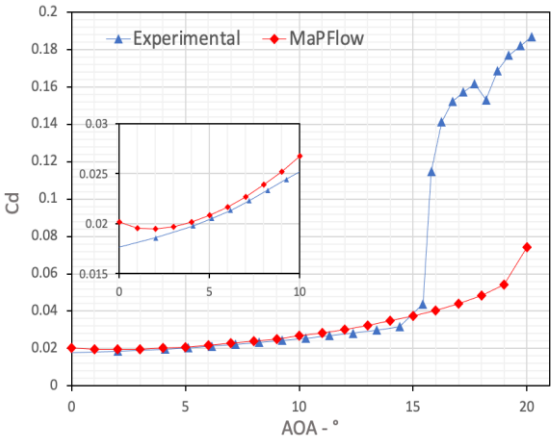

Fig. 3. Drag coefficient variation with angle of attack for the DU97-W-300 airfoil with Vortex Generators. Comparison between the present numerical approach and experimental data from [18].

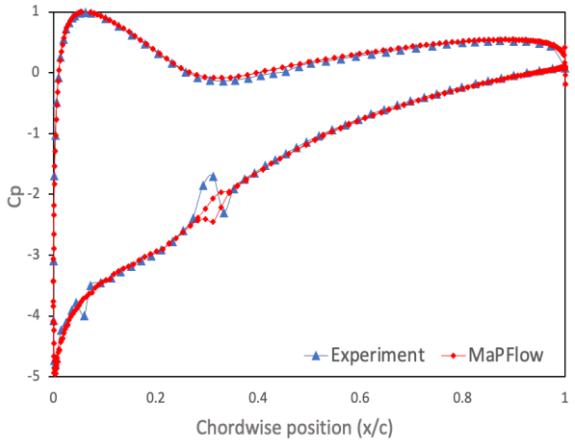

Fig. 4. Pressure coefficient variation attack for the DU97-W-300 airfoil with Vortex Generators at α = 14°. Comparison between the present numerical approach and experimental data from [18].

The effect of the VG vane angle is examined in Fig. 9, Fig. 10 and Fig. 11 where the variation of Lift, Drag and Lift to Drag ratio with angle of attack is shown. In terms of lift, the $\beta = 20°$ performs best, having the highest Cl and smoother post stall behaviour. In terms of Lift to Drag ratio however, the $\beta = 10°$ is a more attractive option, mainly because the drag penalty at lower AoA is minimal.

The VG configuration with the highest increase in $C_{l_{max}}$ and smoother stall ($h = \delta,\ x_{VG} = 20\%\ c$ and $\beta = 20°$) was also tested at two different Re numbers (Re = 0.65×10^6 and Re = 2.0×10^6). The selected Re number limits correspond to the minimum and maximum expected Re numbers of the tidal turbine operational range. Results shown in Fig. 24, Fig. 25 and Fig. 26 indicate an increase in Re number leads to higher $C_{l_{max}}$ and lower drag for the uncontrolled case, as expected. The VG effectiveness increases with Re number, conceivably because the relevant VG height with respect to the local boundary layer increases as well.

For the tidal turbine performance discussed in Section III C, the $h = \delta,\ x_{VG} = 20\%\ c$ and $\beta = 10°$ was selected for the 30% thick hydrofoil profile.

B. VG effect on the 20% Hydrofoil

The effect of the VG chordwise location on the performance of the 20% hydrofoil is given in Fig. 12, Fig. 13 and Fig. 14, in terms of lift, drag and lift to drag ratio, respectively. Similar to wind turbine airfoils of similar thickness, the $x_{VG} = 30\%\ c$ location provides the best results. In terms of VG vane angle, the results shown in Fig. 15, Fig. 16 and Fig. 17, best results are obtained for $\beta = 10°$, as for the 30% hydrofoil. Figures from Fig. 18 to Fig. 21 show the effect of VG height and inter-vane spacing D. Results suggest that VGs higher than the local boundary layer increase the drag penalty significantly while increasing the inter-vane spacing beyond $D = 7$ has a detrimental effect.

The VG configuration with $h = 1.7\delta, x_{VG} = 30\%\ c, \beta = 15°$ was also examined at the two Re numbers extremes, Re = 0.65×10^6 and Re = 2.0×10^6, see Fig. 27, Fig. 28 and Fig. 29. As with the 30% profile, the increase in Re number leads to an increase in VG effectiveness.

For the tidal turbine performance discussed in Section III C, the $h = 1.7\delta,\ x_{VG} = 30\%\ c$ and $\beta = 10°$ was selected for the 20% thick hydrofoil profile.

C. VG effect on the Turbine Performance

Fig. 5 shows the effect the VGs on the predicted turbine power and thrust, as a function of the tip speed ratio (TSR). The VGs lead to increased C_P, especially in the tip speed ratio range of $3 \leq TSR \leq 8$. A maximum increase of 1.2% is observed at $TSR = 3.5$. At this operating point, the flow tends to separate due to the high angles of attack, thus the effect of the VGs is maximal. For the optimal operating point at $TSR_{opt} = 5$, the VGs lead to a 0.5% increase in $C_{P,max}$.

IV. CONCLUSIONS

An in-house RANS solver has been used to perform a computational parametric study of the VG effect on hydrofoil profiles. The results are in good agreement with the existing literature on wind turbine airfoils. The produced force coefficient polars were used as input for an in-house BEM numerical tool, to estimate the effect of the VGs on the turbine performance. The results are promising as there is small increase of the turbine performance at the rated conditions.

The limitations of the study are known. The low aspect ratio VG CFD simulations do not take into account large scale 3D effects such as stall cells [30]. Furthermore, the BEM method is a 2D approximation of the highly 3D flow around a turbine blade and although it accounts for 3D effects at the blade tip and root, the applicability is limited. Future work includes wind tunnel tests of the 20% hydrofoil profile as well as high fidelity Large Eddy Simulations [31] to further validate the VG polars. Also, 3D blade RANS CFD simulations with and without the VGs to validate the BEM results are planned.

At the present stage, the results are promising and indicate that, with suitable design, a flow control method widely applied on wind turbines could be used on tidal turbines as well.

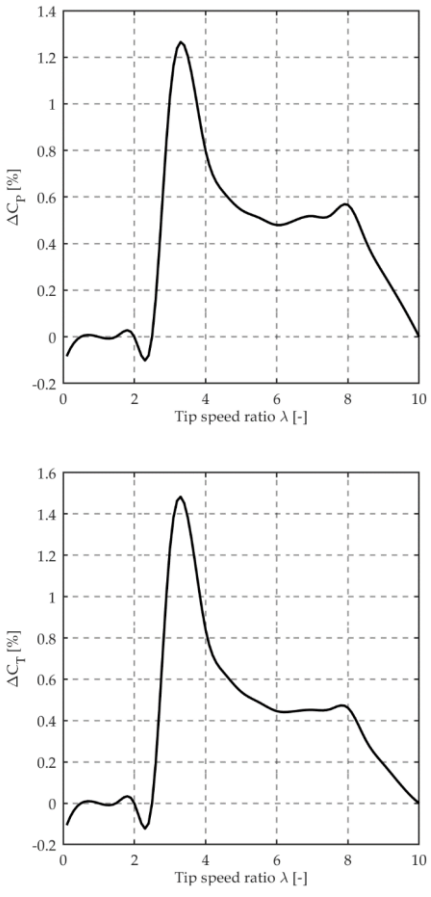

Fig. 5. Relative change of the predicted turbine power (top) and thrust (bottom) coefficient as function of the tip speed ratio due to the effect of VGs on the polar data at the blade root.

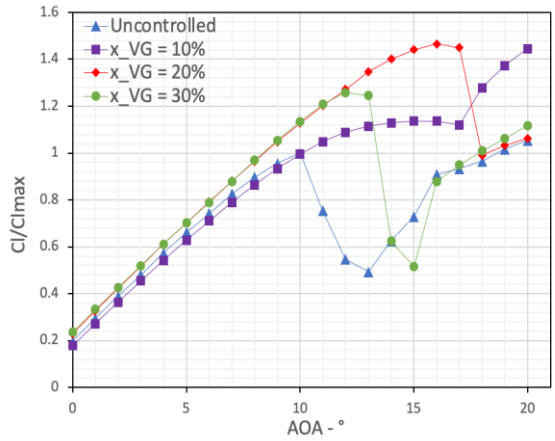

Fig. 6. Lift coefficient variation with AoA for the 30% hydrofoil with and without VGs. VG chordwise location effect for constant VG height and angle: $h = \delta, \beta = 15°$.

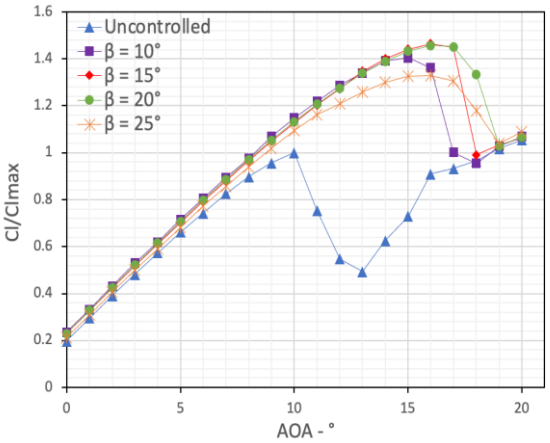

Fig. 9. Lift coefficient variation with AoA for the 30% hydrofoil with and without VGs. VG angle effect for constant VG height and chordwise location: $h = \delta,\ x_{VG} = 20\%\ c$.

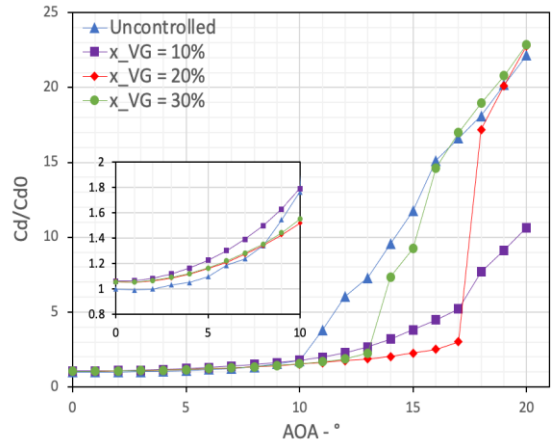

Fig. 7. Drag coefficient variation with AoA for the 30% hydrofoil with and without VGs. VG chordwise location effect for constant VG height and angle: $h = \delta, \beta = 15°$.

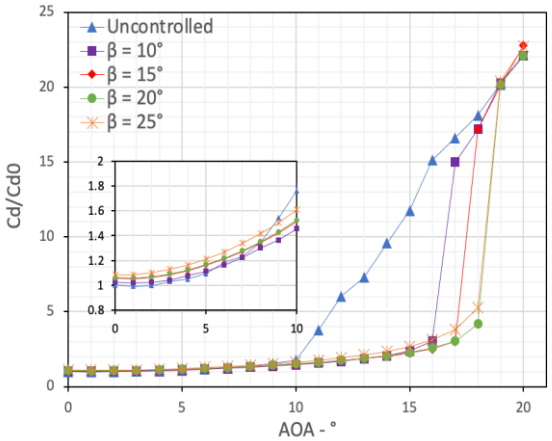

Fig. 10. Drag coefficient variation with AoA for the 30% hydrofoil with and without VGs. VG angle effect for constant VG height and chordwise location: $h = \delta,\ x_{VG} = 20\%\ c$.

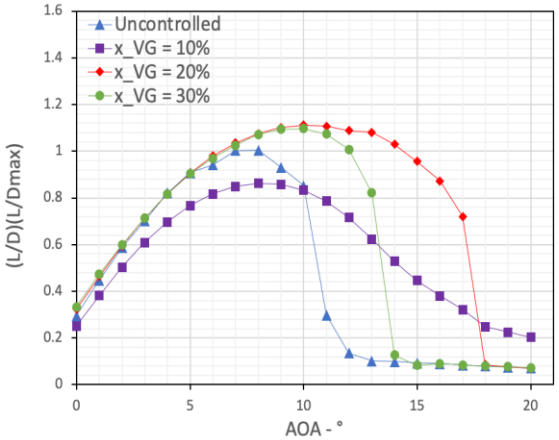

Fig. 8. Lift to drag ratio (L/D) variation with AoA for the 30% hydrofoil with and without VGs. VG chordwise location effect for constant VG height and angle: $h = \delta, \beta = 15°$.

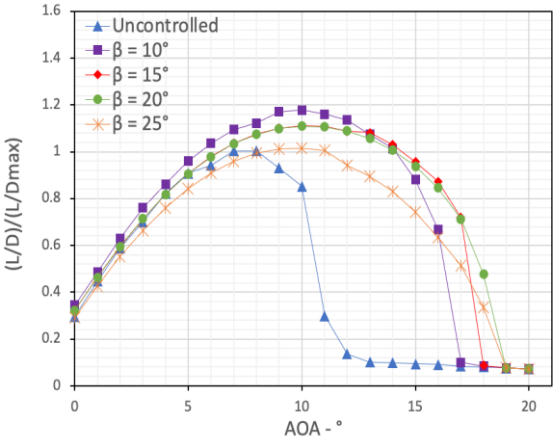

Fig. 11. Lift to drag ratio variation with AoA for the 30% hydrofoil with and without VGs. VG angle effect for constant VG height and chordwise location: $h = \delta,\ x_{VG} = 20\%\ c$.

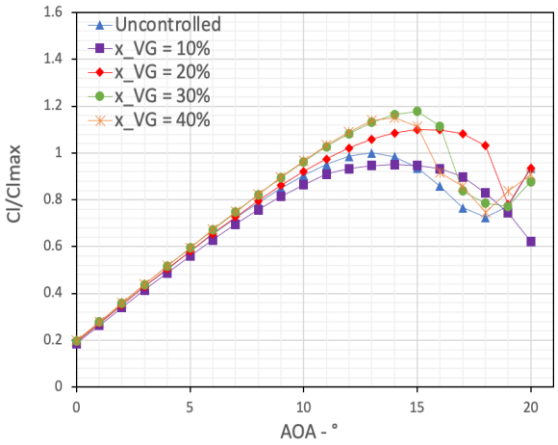

Fig. 12. Lift coefficient variation with AoA for the 20% hydrofoil with and without VGs. VG chordwise location effect for constant VG height and angle: $h = \delta, \beta = 15°$.

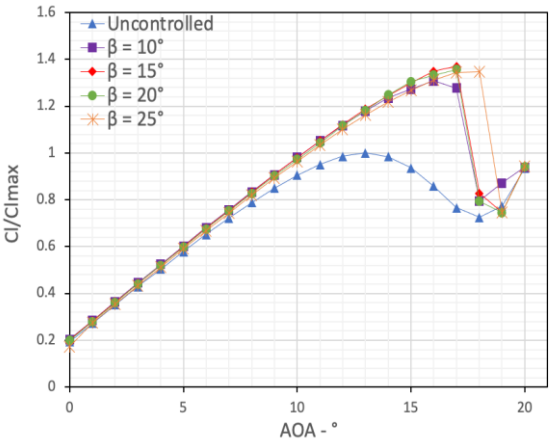

Fig. 15. Lift coefficient variation with AoA for the 20% hydrofoil with and without VGs. VG angle effect for constant VG height and chordwise location: $h = 1.7\delta,\ x_{VG} = 30\%\ c$.

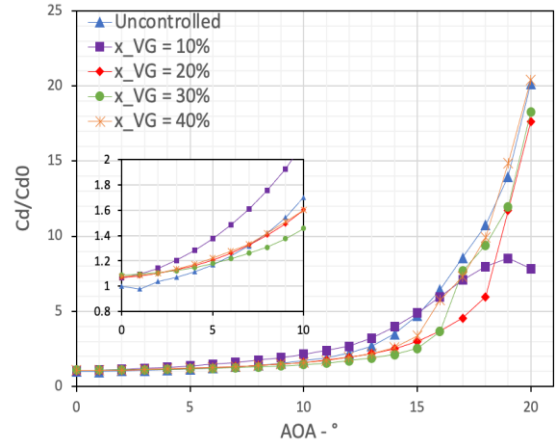

Fig. 13. Drag coefficient variation with AoA for the 20% hydrofoil with and without VGs. VG chordwise location effect for constant VG height and angle: $h = \delta, \beta = 15°$.

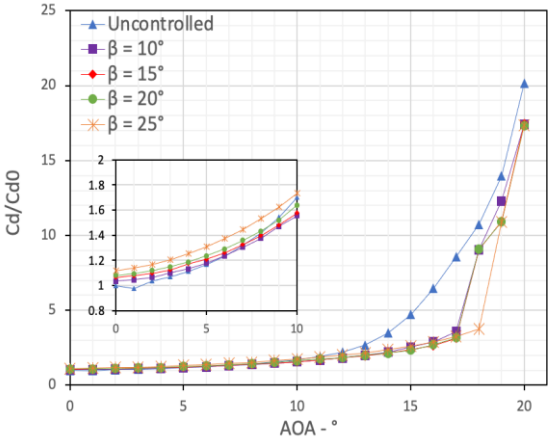

Fig. 16. Drag coefficient variation with AoA for the 20% hydrofoil with and without VGs. VG angle effect for constant VG height and chordwise location: $h = 1.7\delta,\ x_{VG} = 30\%\ c$.

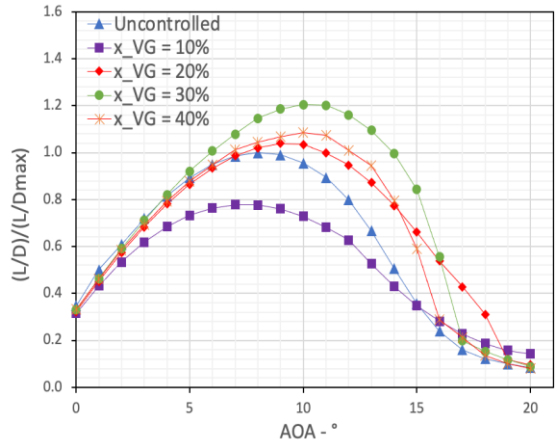

Fig. 14. Lift to drag ratio (L/D) coefficient variation with AoA for the 20% hydrofoil with and without VGs. VG chordwise location effect for constant VG height and angle: $h = \delta, \beta = 15°$.

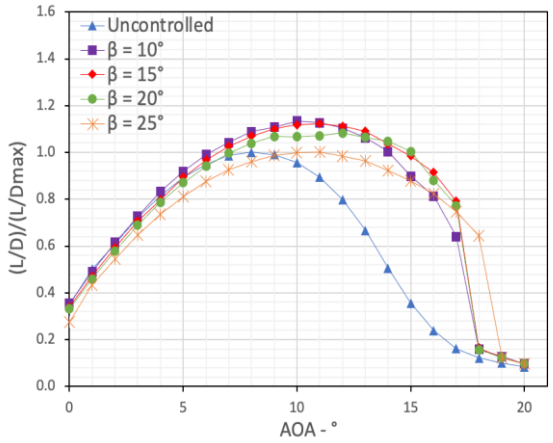

Fig. 17. Lift to drag ratio coefficient variation with AoA for the 20% hydrofoil with and without VGs. VG angle effect for constant VG height and chordwise location: $h = 1.7\delta,\ x_{VG} = 30\%\ c$.

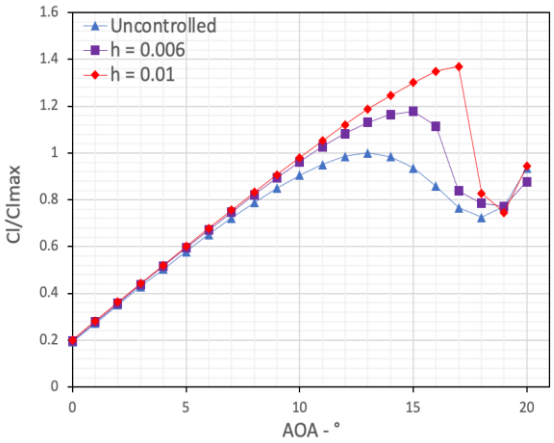

Fig. 18. Lift coefficient variation with AoA for the 20% hydrofoil with and without VGs. VG height effect for constant VG chordwise location and angle: $x_{VG} = 30\%\ c, \beta = 15°$.

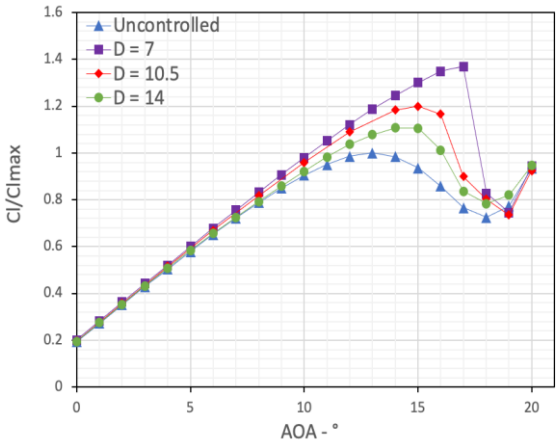

Fig. 21. Lift coefficient variation with AoA for the 20% hydrofoil with and without VGs. VG inter-vane spacing (D) effect for constant VG chordwise location, height and angle: $x_{VG} = 30\%\ c, h = \delta, \beta = 15°$.

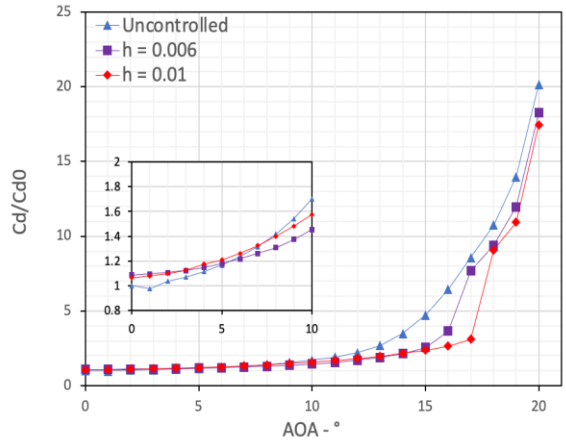

Fig. 19. Drag coefficient variation with AoA for the 20% hydrofoil with and without VGs. VG height effect for constant VG chordwise location and angle: $x_{VG} = 30\%\ c, \beta = 15°$.

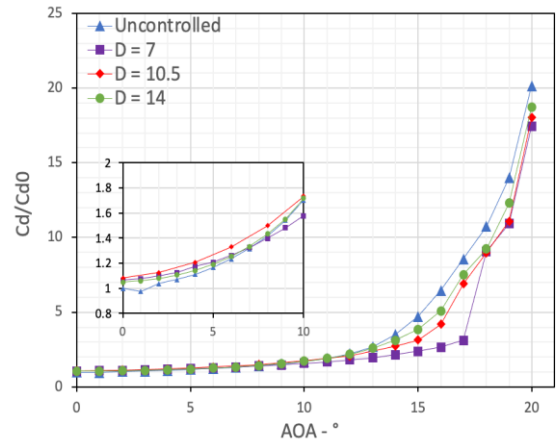

Fig. 22. Drag coefficient variation with AoA for the 20% hydrofoil with and without VGs. VG inter-vane spacing (D) effect for constant VG chordwise location, height and angle: $x_{VG} = 30\%\ c, h = \delta, \beta = 15°$.

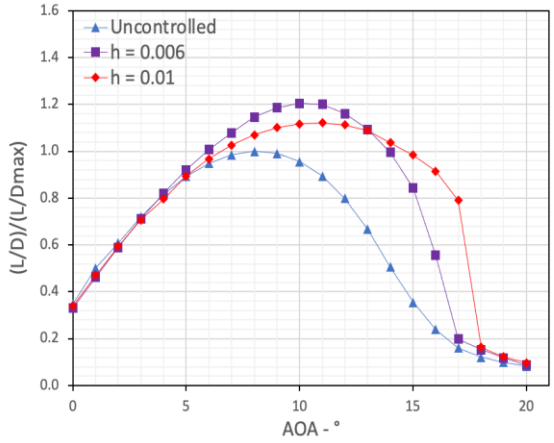

Fig. 20. Lift to drag ratio (L/D) variation with AoA for the 20% hydrofoil with and without VGs. VG height effect for constant VG chordwise location and angle: $x_{VG} = 30\%\ c, \beta = 15°$.

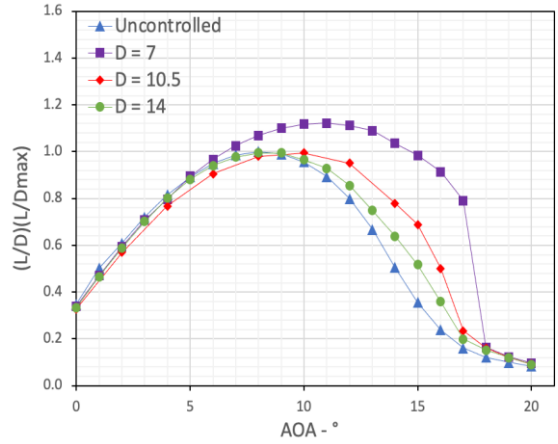

Fig. 23. Lift to drag (L/D) variation with AoA for the 20% hydrofoil with and without VGs. VG inter-vane spacing (D) effect for constant VG chordwise location, height and angle: $x_{VG} = 30\%\ c, h = \delta, \beta = 15°$.

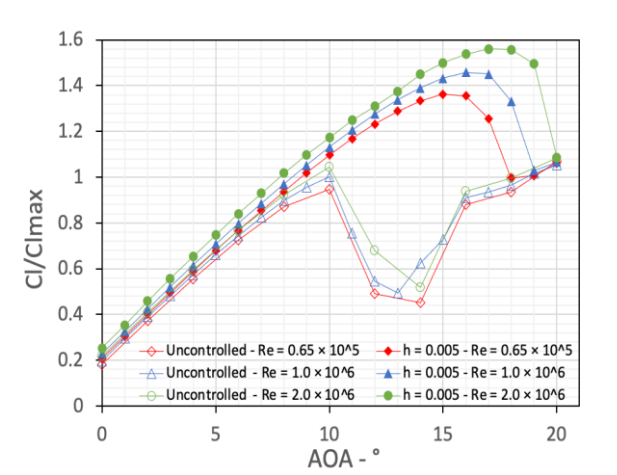

Fig. 24. Lift coefficient variation with AoA for the 30% hydrofoil with and without VGs. Reynolds number effect for constant VG height, chordwise location and angle: $h = 0.005\ c$, $x_{VG} = 20\%\ c, \beta = 20°$.

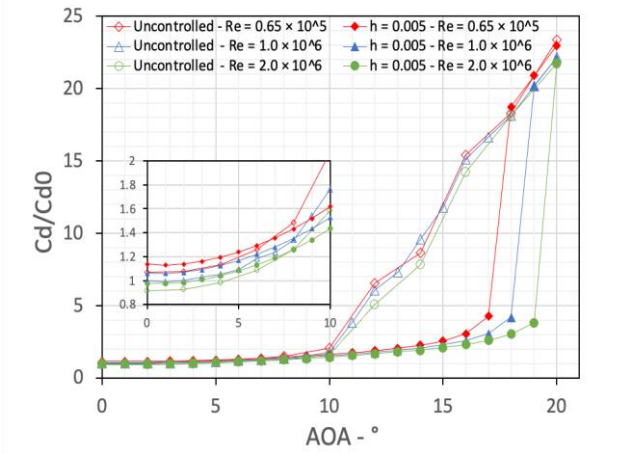

Fig. 25. Drag coefficient variation with AoA for the 30% hydrofoil with and without VGs. Reynolds number effect for constant VG height, chordwise location and angle: $h = 0.005\ c, x_{VG} = 20\%\ c, \beta = 20°$.

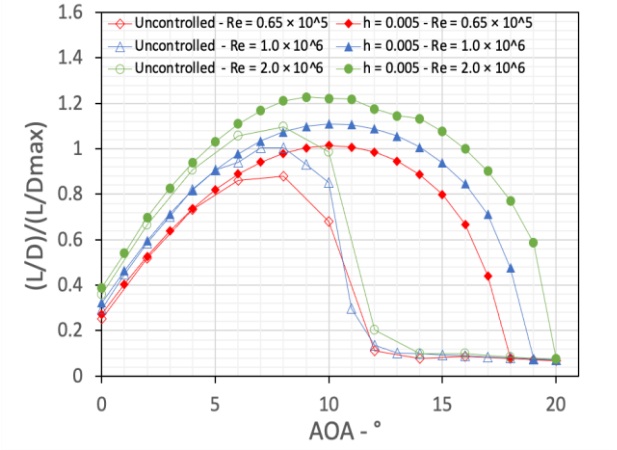

Fig. 26. Drag coefficient variation with AoA for the 30% hydrofoil with and without VGs. Reynolds number effect for constant VG height, chordwise location and angle: $h = 0.005\ c, x_{VG} = 20\%\ c, \beta = 20°$.

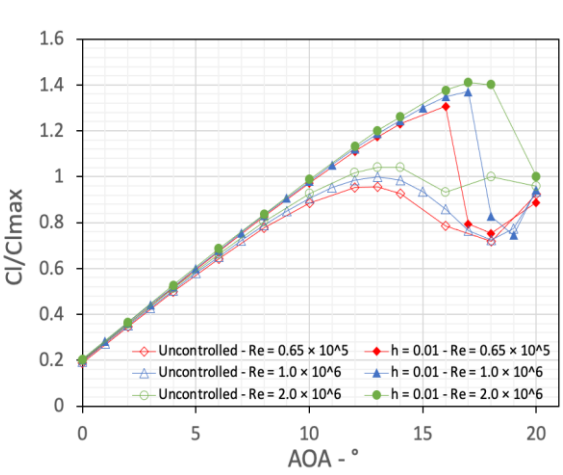

Fig. 27. Lift coefficient variation with AoA for the 20% hydrofoil with and without VGs. Reynolds number effect for constant VG height, chordwise location and angle: $h = 0.010\ c$, $x_{VG} = 30\%\ c, \beta = 15°$.

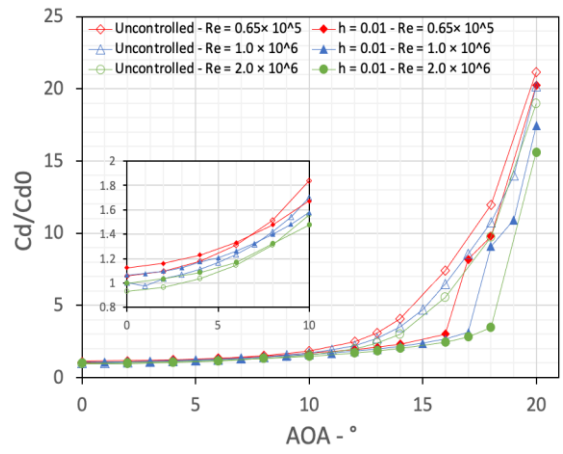

Fig. 28. Drag coefficient variation with AoA for the 20% hydrofoil with and without VGs. Reynolds number effect for constant VG height, chordwise location and angle: $h = 0.010\ c$, $x_{VG} = 30\%\ c, \beta = 15°$.

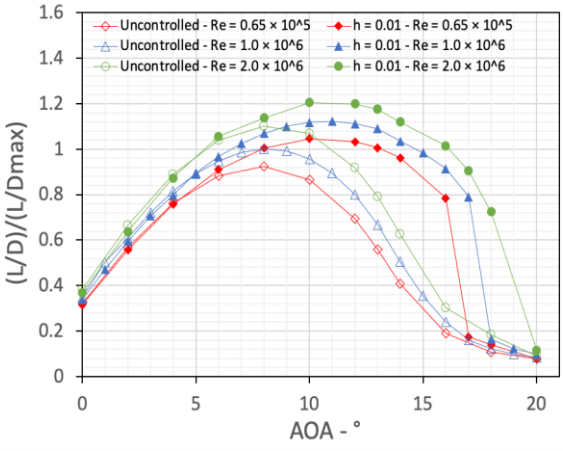

Fig. 29. Drag coefficient variation with AoA for the 20% hydrofoil with and without VGs. Reynolds number effect for constant VG height, chordwise location and angle: $h = 0.010\ c$, $x_{VG} = 30\%\ c, \beta = 15°$.

REFERENCES

[1] W. Shi, D. Wang, M. Atlar, and K.-C. Seo, "Flow separation impacts on the hydrodynamic performance analysis of a marine current turbine using CFD," *Proc. Inst. Mech. Eng. Part A J. Power Energy*, vol. 227, no. 8, pp. 833–846, Dec. 2013, doi: 10.1177/0957650913499749.

[2] W. Skrzypiński, M. Gaunaa, and C. Bak, "The effect of mounting vortex generators on the dtu 10mw reference wind turbine blade," in *Journal of Physics: Conference Series*, Jun. 2014, vol. 524, p. 12034, doi: 10.1088/1742-6596/524/1/012034.

[3] J. C. Lin, "Control of turbulent boundary-layer separation using micro-vortex generators," *AIAA Pap.*, no. 99–993404, 1999.

[4] S. Øye, "The effect of vortex generators on the performance of the Elkraft 1000 kW turbine," 1995.

[5] G. Thomas Scarlett and I. M. Viola, "Unsteady hydrodynamics of tidal turbine blades," *Renew. Energy*, vol. 146, pp. 843–855, Feb. 2020, doi: 10.1016/j.renene.2019.06.153.

[6] I. Afgan, J. McNaughton, S. Rolfo, D. D. Apsley, T. Stallard, and P. Stansby, "Turbulent flow and loading on a tidal stream turbine by LES and RANS," *Int. J. Heat Fluid Flow*, vol. 43, pp. 96–108, Oct. 2013, doi: 10.1016/j.ijheatfluidflow.2013.03.010.

[7] P. Kundu, A. Sarkar, and V. Nagarajan, "Improvement of performance of S1210 hydrofoil with vortex generators and modified trailing edge," *Renew. Energy*, vol. 142, pp. 643–657, Nov. 2019, doi: 10.1016/j.renene.2019.04.148.

[8] G. Papadakis and S. G. Voutsinas, "A strongly coupled Eulerian Lagrangian method verified in 2D external compressible flows," *Comput. Fluids*, vol. 195, p. 104325, Dec. 2019, doi: 10.1016/j.compfluid.2019.104325.

[9] F. R. Menter, "Zonal two equation k-w turbulence model for aerodynamic flows," *AIAA Pap.*, no. 1993–2906, 1993, doi: 10.2514/6.1993-2906.

[10] E. E. Bender, B. H. Anderson, and P. J. Yagle, "Vortex generator modeling for Navier-Stokes codes," *ASME Pap. FEDSM99-6919*, 1999.

[11] A. Jirasek, "Vortex-Generator Model and Its Application to Flow Control," *J. Aircr.*, vol. 42, no. 6, pp. 1486–1491, 2005, doi: 10.2514/1.12220.

[12] M. Manolesos, G. Papadakis, and S. G. Voutsinas, "On the Application of the Bay Model for Vortex Generator Flows," 2018, doi: 10.1115/GT2018-75217.

[13] M. Manolesos, G. Papadakis, and S. G. G. Voutsinas, "Revisiting the assumptions and implementation details of the BAY model for vortex generator flows," *Renew. Energy*, vol. 146, pp. 1249–1261, Feb. 2020, doi: 10.1016/j.renene.2019.07.063.

[14] M. Manolesos, G. Papadakis, and S. G. Voutsinas, "Assessment of the CFD capabilities to predict aerodynamic flows in presence of VG arrays," *J. Phys. Conf. Ser.*, vol. 524, no. 1, p. 012029, Jun. 2014, doi: 10.1088/1742-6596/524/1/012029.

[15] D. Baldacchino *et al.*, "Experimental benchmark and code validation for airfoils equipped with passive vortex generators," *J. Phys. Conf. Ser.*, vol. 753, no. 2, p. 022002, Sep. 2016, doi: 10.1088/1742-6596/753/2/022002.

[16] M. Manolesos, N. N. Sørensen, N. Troldborg, L. Florentie, G. Papadakis, and S. Voutsinas, "Computing the flow past Vortex Generators: Comparison between RANS Simulations and Experiments," *J. Phys. Conf. Ser.*, vol. 753, no. 2, p. 022014, Sep. 2016, doi: 10.1088/1742-6596/753/2/022014.

[17] M. Manolesos, "Experimental and computational study of three-dimensional separation and separation control using passive vortex generators," NTUA, PhD Thesis, Athens, 2013.

[18] D. Baldacchino, C. Ferreira, D. De Tavernier, W. A. Timmer, and G. J. W. van Bussel, "Experimental parameter study for passive vortex generators on a 30% thick airfoil," *Wind Energy*, vol. 21, no. 9, pp. 745–765, Sep. 2018, doi: 10.1002/we.2191.

[19] M. Manolesos and S. G. Voutsinas, "Experimental investigation of the flow past passive vortex generators on an airfoil experiencing three-dimensional separation," *J. Wind Eng. Ind. Aerodyn.*, vol. 142, pp. 130–148, Jul. 2015, doi: 10.1016/j.jweia.2015.03.020.

[20] M. Manolesos, G. Papadakis, and S. Voutsinas, "An experimental and numerical investigation on the formation of stall-cells on airfoils," *J. Phys. Conf. Ser.*, vol. 555, no. 1, p. 012068, Dec. 2014, doi: 10.1088/1742-6596/555/1/012068.

[21] M. Manolesos, G. Papadakis, and S. G. Voutsinas, "Experimental and computational analysis of stall cells on rectangular wings," *Wind Energy*, vol. 17, no. 6, pp. 939–955, Jun. 2014, doi: 10.1002/we.1609.

[22] R. Soto-Valle, S. Bartholomay, C. N. Nayeri, C. O. Paschereit, and M. Manolesos, "Airfoil shaped vortex generators applied on a research wind turbine," 2021.

[23] N. Kaufmann, T. H. Carolus, and R. Starzmann, "An enhanced and validated performance and cavitation prediction model for horizontal axis tidal turbines," *Int. J. Mar. Energy*, vol. 19, pp. 145–163, Sep. 2017, doi: 10.1016/j.ijome.2017.07.003.

[24] M. L. Buhl, "A New Empirical Relationship between Thrust Coefficient and Induction Factor for the Turbulent Windmill State, Technical Report: NREL/TP-500-36834," 2005. Accessed: Apr. 09, 2021. [Online]. Available: http://www.osti.gov/bridge.

[25] H. Glauert, "Airplane propellers," in *Aerodynamic theory*, vol. 4, Springer, 1935, pp. 169–360.

[26] W. Z. Shen, R. Mikkelsen, J. N. Sørensen, and C. Bak, "Tip loss corrections for wind turbine computations," *Wind Energy*, vol. 8, no. 4, pp. 457–475, Oct. 2005, doi: 10.1002/we.153.

[27] L. A. Viterna and R. D. Corrigan, "Fixed pitch rotor performance of large horizontal axis wind turbines," 1981, Accessed: Apr. 09, 2021. [Online]. Available: https://ntrs.nasa.gov/citations/19830010962.

[28] R. Starzmann, I. Goebel, and P. Jeffcoate, "Field Performance Testing of a Floating Tidal Energy Platform-Part 1: Power Performance," 2018.

[29] P. Jeffcoate and N. Cresswell, "Field Performance Testing of a Floating Tidal Energy Platform-Part 2: Load Performance," 2018.

[30] M. Manolesos and S. G. Voutsinas, "Study of a stall cell using stereo particle image velocimetry," *Phys. Fluids*, vol. 26, no. 4, p. 045101, Apr. 2014, doi: 10.1063/1.4869726.

[31] P. Ouro, M. Harrold, T. Stoesser, and P. Bromley, "Hydrodynamic loadings on a horizontal axis tidal turbine prototype," *J. Fluids Struct.*, vol. 71, pp. 78–95, May 2017, doi: 10.1016/j.jfluidstructs.2017.03.009.